Numerical simulation of fracture and damage in RC structures due to fire

J.Cervenka
Cervenka Consulting, Prague, Czech Republic

J. Surovec, P. Kabele
Dep. of Structural Mechanics, Faculty of Civil Engineering, Czech Technical University, Prague, Czech Republic

T. Zimmerman, A. Strauss, K. Bergmeister
Dep. of Structural Engineering and Natural Hazards, Institute for Structural Engineering, University of Natural Resources and Applied Life Sciences, Vienna

ABSTRACT: Paper describes results achieved during a 4 year European research project UPTUN GRD1-2001-40739, which finished in 2006. The objective of the project was to develop new methods and procedures for upgrading European tunnels and increasing their safety against fire accidents. Within the framework of this project authors contributed by developing and extending existing fracture-plastic material models for numerical modelling of structural behaviour subjected to fire. The behaviour of the model is demonstrated on simple uni-axial tests as well as on a three-dimensional analysis of a tunnel fire.

1 INTRODUCTION

Concrete behaviour at high temperature represents a complex phenomenon that in general case requires a coupled hygro-thermo-chemo-mechanical model. An example of an advanced hygro-thermo-mechanical model is presented in Gawin, D. et. al. 2003. This paper presents a modification of the combined fracture-plastic model developed by the authors and initially presented in Cervenka. J. et. al. 1998. The extended model is applied for the analysis of structures subjected to fire, where the material properties of concrete as well as reinforcement are strongly dependent on temperature. The objective is to develop a model that can be applied to large-scale analyses of engineering problems at a reasonable computational cost. The presented work is an extension of a previously published thermally dependent model by Cervenka J. et. al. 2006. The paper presents new results and an application to a real tunnel scenario.

The temperature distribution inside a heated structure is calculated by a separate non-linear transient thermal analysis. The obtained temperature fields are then applied in a mechanical analysis, which takes into account the thermally induced strains as well as the material degradation induced by high temperatures.

The model was developed during the European research project UPTUN. The model behaviour is tested on uni-axial tensile and compression tests as well as on experimental data of a real scale fire experiment of a tunnel suspended ceiling. At the end of the paper the model is applied to investigate the effects of fire resistant shotcrete protection during a Virgolo tunnel fire test.

The temperature dependent mechanical model is implemented in program ATENA (see ATENA 2005). This program was also used to analyse the examples presented in this paper.

2 THERMAL ANALYSIS

Temperature fields for the mechanical analysis are determined by a separate thermal analysis.

$$C_T \frac{\partial T}{\partial t} = -div(J_T), \text{ where } J_T = -K_T grad(T) \qquad (1)$$

In the above standard diffusion formula, T denotes temperature and t represents time. C_T and K_T are thermal capacity and conductivity respectively. Both capacity and conductivity are functions of current temperature. A modified Crank-Nicholson integration scheme (Wood, W.L. 1990, Jendele, L. 2001) is used to integrate the non-linear set of equations. The resulting iterative correction of unknown temperatures $\Delta\psi$ at time $t+\Delta t$ is calculated by the following formula:

$$\Delta\psi = \left(\tilde{\mathbf{K}}\right)^{-1} \tilde{J} \qquad (2)$$

where:

$$\tilde{\mathbf{K}} = \left(\mathbf{K}\theta + \frac{1}{\Delta t}\mathbf{C}\right)$$

$$\tilde{J} = \bar{J} - \mathbf{K}\left(\theta\, {}^{t+\Delta t}\psi + (1-\theta)\, {}^{t}\psi\right) - \mathbf{C}\frac{1}{\Delta t}\left({}^{t+\Delta t}\psi - {}^{t}\psi\right)$$

$\mathbf{C}$ and $\mathbf{K}$ are capacity and conductivity matrices respectively after spatial discretization by finite element method. θ is the integration parameter. For

$\theta = 0.5$ the Crank-Nicholson formulation is recovered. $\theta = 0$ corresponds to the Euler explicit scheme, and the Euler implicit formulation is obtained when $\theta = 1$. The known oscillatory behaviour of the Crank-Nicholson formulation is addressed by introducing the following iterative damping (Jendele, L. 2001).

$$^{t+\Delta t}\underline{\psi} = ^{t+\Delta t(i)}\underline{\psi} = ^{t+\Delta t(i-1)}\underline{\psi} + ^{t+\Delta t(i)}\eta\,\Delta\underline{\psi} \qquad (3)$$

The recommended value of the damping parameter η is in the interval of $\langle 0.3;1 \rangle$.

3 MATERIAL MODEL FOR CONCRETE

The concrete mechanical model follows the original theory in Cervenka at al. 1998. The material model formulation is based on the strain decomposition into elastic ε_{ij}^{e}, plastic ε_{ij}^{p} and fracturing ε_{ij}^{f} components (de Borst, R. 1986).

$$\varepsilon_{ij} = \varepsilon_{ij}^{e} + \varepsilon_{ij}^{p} + \varepsilon_{ij}^{f} \qquad (1)$$

The new stress state is then computed by the formula:

$$\sigma_{ij}^{n} = \sigma_{ij}^{n-1} + E_{ijkl}(\Delta\varepsilon_{kl} - \Delta\varepsilon_{kl}^{p} - \Delta\varepsilon_{kl}^{f}) \qquad (2)$$

Tensile behaviour of concrete is modelled by non-linear fracture mechanics with a simple Rankine based criterion.

$$F_{i}^{f} = \sigma_{i}'^{t} - f_{ti}'(w_{i}') \le 0 \qquad (3)$$

In this method the smeared crack concept is accepted. Its parameters are: tensile strength f_t, shape of the stress-crack opening curve $f_t(w)$ and fracture energy G_F. It is assumed that strains and stresses are converted into the material directions, which in case of rotated crack model correspond to the principal stress directions, and in case of fixed crack model, are given by the principal directions at the onset of cracking. Therefore, $\sigma_i'^{t}$ identifies the trial stress and f_{ti}' tensile strength in the material direction i. The prime symbol denotes quantities in the material directions. This approach is combined with the crack band method of Bažant, Z.P. & Oh, B.H. 1983. In this formulation, the cracking strain is related to the element size. Consequently, the softening law in terms of strains for the smeared model is calculated for each element individually, while the crack-opening law is preserved. The model uses an exponential softening law of Hordijk 1991.

Compressive behaviour is modelled using a plasticity-based model with failure surface defined by Menetrey, P. & Willam, K.J. 1995 three-parameter criterion

$$F_{3P}^{p} = \left[\sqrt{1.5}\,\frac{\rho}{f_c}\right]^2 + m\left[\frac{\rho}{\sqrt{6}f_c}r(\theta,e) + \frac{\xi}{\sqrt{3}f_c}\right] - c = 0 \qquad (4)$$

where

$$m = 3\frac{f_c^2 - f_t^2}{f_c\,f_t}\frac{e}{e+1},$$

$$r(\theta,e) = \frac{4(1-e^2)\cos^2\theta + (2e-1)^2}{2(1-e^2)\cos\theta + (2e-1)\left[4(1-e^2)\cos^2\theta + 5e^2 - 4e\right]^{\frac{1}{2}}}$$

In the above equations, (ξ,ρ,θ) are Heigh-Vestergaard coordinates, and f_c and f_t are compressive strength and tensile strength respectively. Parameter $e \in \langle 0.5,1.0 \rangle$ defines the roundness of the failure surface.

The surface evolves during the yielding/crushing process by the hardening/softening laws based on equivalent plastic strain defined as:

$$\Delta\varepsilon_{eq}^{p} = \min(\Delta\varepsilon_{i}^{p}) \qquad (5)$$

Hardening $\varepsilon_{eq}^{p} \in \langle -\varepsilon_{c}^{p};0 \rangle$:

$$f_c(\varepsilon_{eq}^{p}) = f_{co} + (f_c - f_{co})\sqrt{1 - \left(\frac{\varepsilon_{c}^{p} - \varepsilon_{eq}^{p}}{\varepsilon_{c}^{p}}\right)^2} \qquad (6)$$

Softening $\varepsilon_{eq}^{p} \in \langle -\infty;-\varepsilon_{c}^{p} \rangle$:

$$c = \left(1 - \frac{w_c}{w_d}\right)^2, \qquad w_c \in \langle -w_d;0 \rangle$$

$$c = 0, \qquad w_c \in (-\infty;w_d) \qquad (7)$$

$$w_c = (\varepsilon_{eq}^{p} - \varepsilon_{c}^{p})\,L_c \qquad (8)$$

When crushing enters into the softening regime, an analogous approach to the crack band model is used also for the localization in compression within the crushing band L_c. A direct return-mapping algorithm is used to solve the predictor-corrector equation of the plasticity model.

$$F^{p}(\sigma_{ij}^{t} - \sigma_{ij}^{p}) = F^{p}(\sigma_{ij}^{t} - \Delta\lambda l_{ij}) = 0 \qquad (9)$$

The plastic stress σ_{ij}^{p} is a product of plastic multiplier $\Delta\lambda$ and the return direction l_{ij}, which is defined as

$$l_{ij} = E_{ijkl}\frac{\partial G^{p}(\sigma_{kl}^{t})}{\partial\sigma_{kl}} \text{ then} \qquad \Delta\varepsilon_{ij}^{p} = \Delta\lambda\frac{\partial G^{p}(\sigma_{ij}^{t})}{\partial\sigma_{ij}} \qquad (10)$$

Plastic potential G^p is given by:

$$G^{p}(\sigma_{ij}) = \beta\frac{1}{\sqrt{3}}I_1 + \sqrt{2J_2} \qquad (11)$$

where β determines the return direction. If $\beta < 0$, material is being compacted during crushing, if $\beta = 0$, the material volume is preserved, and if $\beta > 0$, the material is dilating.

A special iterative algorithm analogous to multi-surface plasticity is used to solve the plastic and

fracture models such that the final stress tensors in both models are identical. This algorithm is schematically shown in two-dimensions in Figure 1.

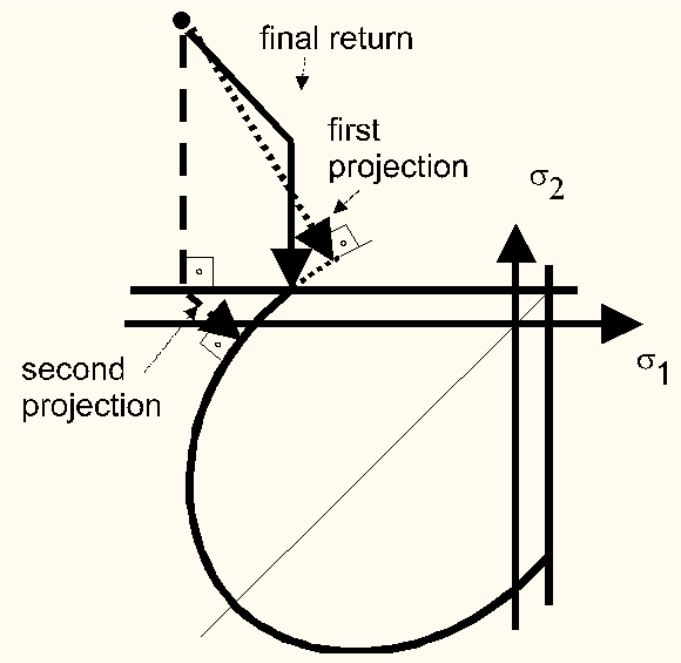

Figure 1. Iterative algorithm for solving interaction of fracture-plastic surfaces (for simplicity shown in 2D).

4 MATERIAL MODEL FOR REINFORCEMENT

Finite element modelling of reinforced concrete structures requires special tools for modelling of all types of reinforcement (Jendele & Cervenka 2006).

Concrete is modelled by solid elements. Interface material models can model frictional contacts between structural parts. The mesh type of reinforcement can be represented as smeared reinforcement. In this approach, the individual bars are not considered, while reinforcement is modelled as a component of a general composite material.

Individual bars can be modelled by truss elements embedded in concrete elements with axial stiffness only. In this technique, the mesh is generated first for concrete. Then the bar elements are embedded into each solid element. The bar elements are then connected to the solid model by special constrain conditions. These conditions represent a kinematic dependence of reinforcement displacements on those of concrete nodes. Thus the reinforcing does not affect the mesh generation. The described family of finite elements makes it possible to cover most practical cases of reinforced concrete structures.

5 TEMPERATURE DEPENDENT MATERIAL PROPERTIES

The material models for concrete as well as reinforcement are formulated in a purely incremental manner, and the selected material parameters are temperature dependent. The temperature dependent evolution laws of these parameters are shown in subsequent figures. They have been derived based on Eurocode 2 and by matching experimental results of Castillo, C. & Durani, A.J. 1990. An analogous dependence is used also for the stress-strain law for reinforcement. The stress-strain diagram is scaled based on the highest reached temperature at each reinforcement element according to the Eurocode 2 formulas.

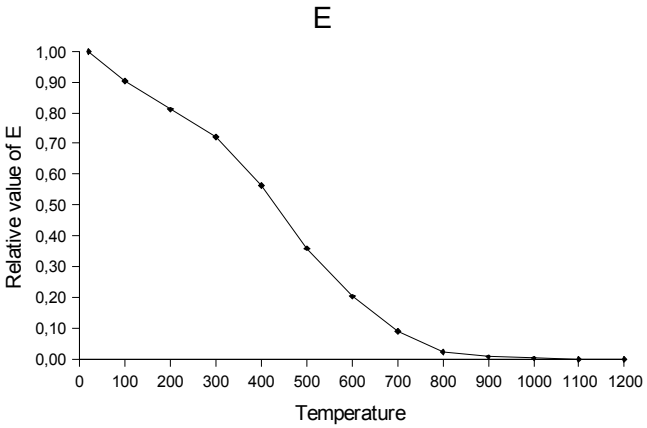

Figure 2. Temperature dependence of concrete E modulus.

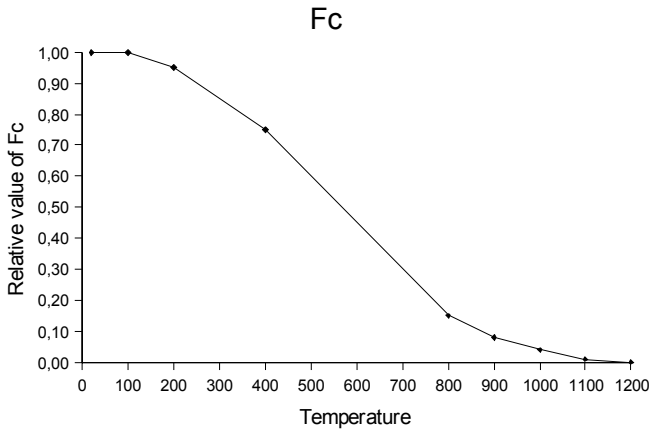

Figure 3. Temperature dependence of concrete compressive strength.

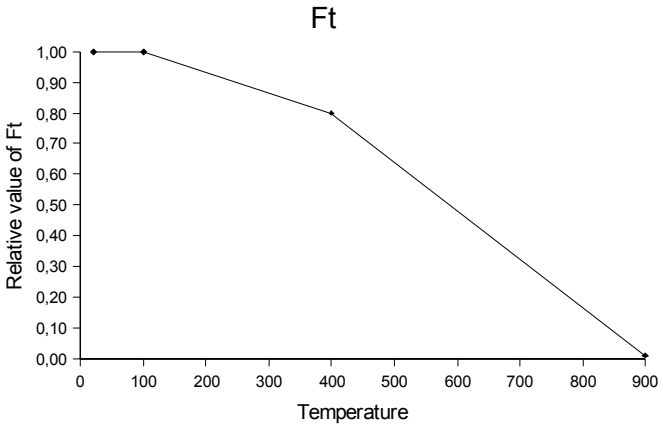

Figure 4. Temperature dependence of concrete tensile strength.

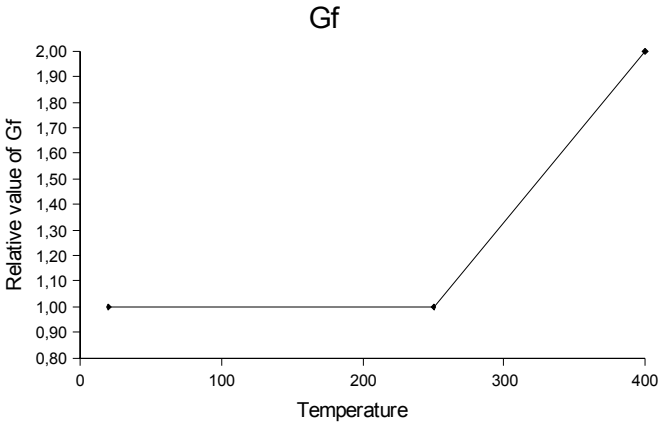

Figure 5. Temperature dependence of fracture energy.

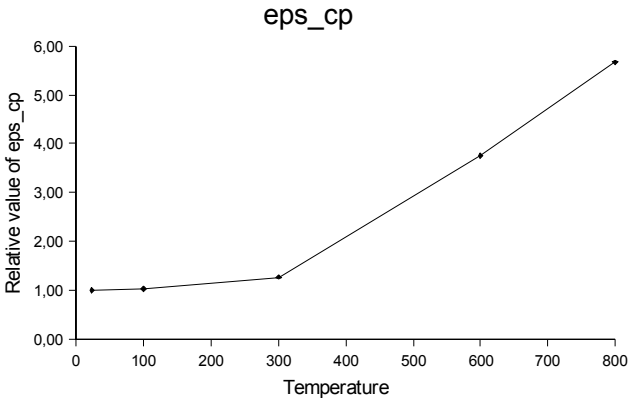

Figure 6. Temperature dependence of plastic strain at compressive strength (see Eq. (6)).

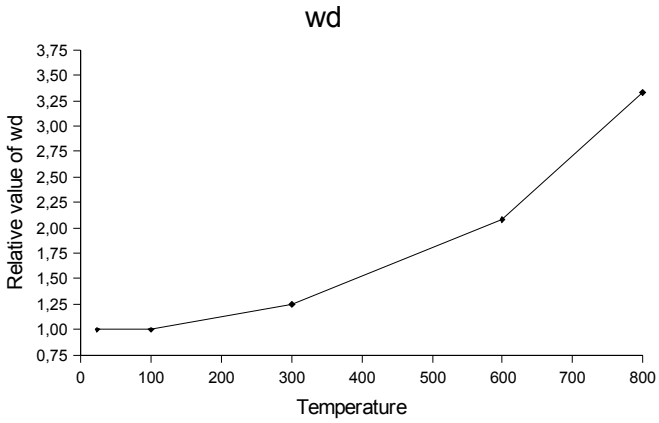

Figure 7. Temperature dependence of critical crushing displacement (see Eq. (7))

6 EXAMPLES AND VALIDATION

Several examples are presented to demonstrate the behaviour of the proposed model on simple uniaxial tests as well as on a more complicated example of a tunnel suspended ceiling subjected to fire.

6.1 *Uniaxial tests*

Standard compression and tensile tests were simulated, in which the specimen was loaded to collapse under uniform temperature field distribution. The temperatures chosen ranged from 100°C to 800 °C with a step of 100 °C and they correspond to the test data published in Castillo, C. & Durani, A.J. 1990. The results show the behaviour of the material model at various temperature levels and are depicted in Figure 8 and Figure 9.

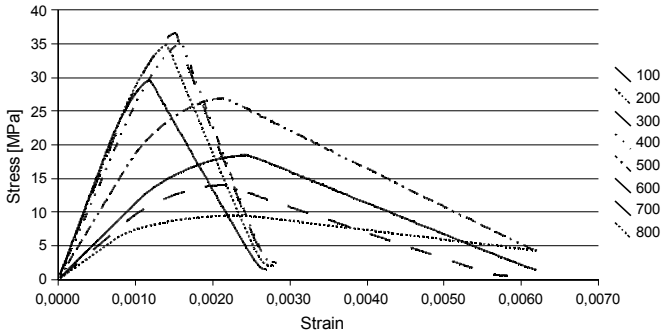

Figure 8. Uniaxial compression tests.

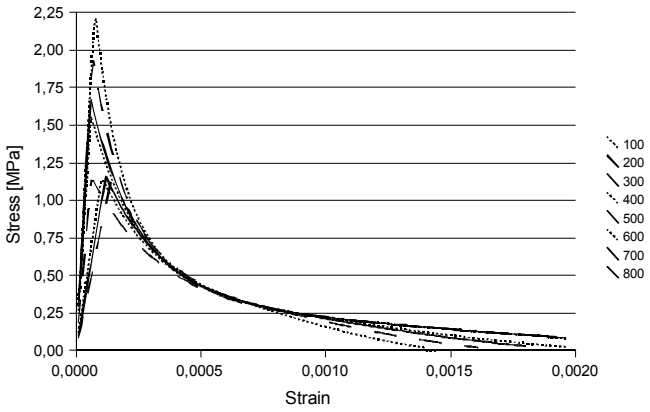

Figure 9. Uniaxial tension tests.

6.2 *Suspended ceiling simulation*

The structure consisted of a reinforced concrete suspended ceiling slab with a total span of 8.0 m, suspended in the mid-span by a pair of hangers. The geometry corresponds to a specimen, which was tested during a European research project UPTUN. The thickness of the slab is 200 mm and the width is 2.0 m. The geometry of the specimen represents a suspended ceiling in a typical concrete tunnel such as is shown in Figure 10.

The symmetry of the structure is taken advantage of, so that the model in Figure 11 consists of one quarter of the structure. The deformed mesh is shown in Figure 13, and it contains 8827 nodes and 6595 linear iso-parametric brick elements.

The structure was exposed to a pool fire along the bottom part of the ceiling structure. The maximum temperature 1100 °C was reached along the bottom surface during the experiment. In the analysis, however, uniform temperature was considered along the bottom face of the slab by averaging the values measured in the experiment (see Figure 12). No

thermal shielding was considered. The structure was initially loaded with assumed self weight of 5 kN/m^2 and a live load of 3.5 kN/m^2, and then the fire actions were applied.

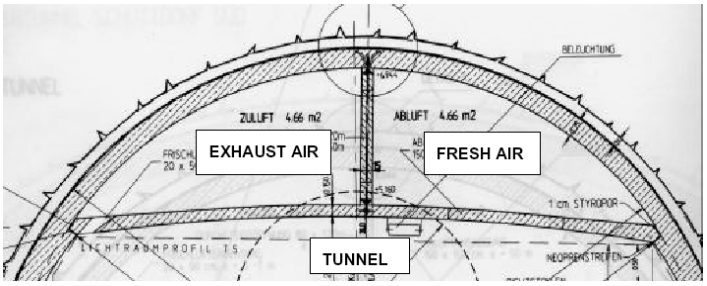

Figure 10. Typical tunnel cross-section with a suspended reinforced concrete ceiling.

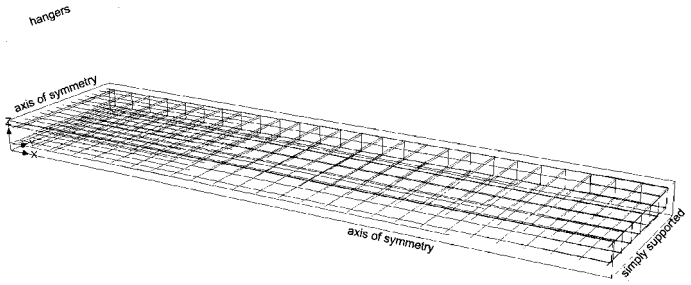

Figure 11. Three-dimensional model of a quarter of the suspended ceiling.

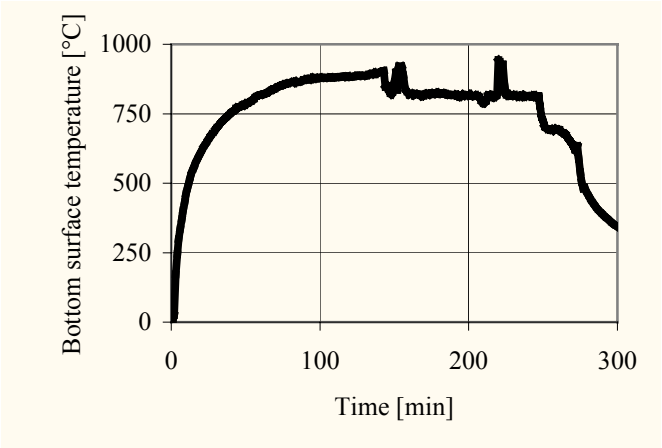

Figure 12. Average bottom surface temperature in the experiment.

First transient thermal analysis was performed with temperature dependent material properties. Then the obtained thermal fields were used in subsequent incremental stress analysis

The subsequent figures show the main results obtained in this study. Figure 14 compares the mid-span deflections. The figure shows that a good prediction was obtained for the maximum deflection, however the deflections for times around 60 minutes were overestimated by almost 50%. The analyses showed that the main parameter affecting the deflection results is the thermal expansion. Good agreement was obtained in the case of 3D analysis with the adjusted law for free thermal strain.

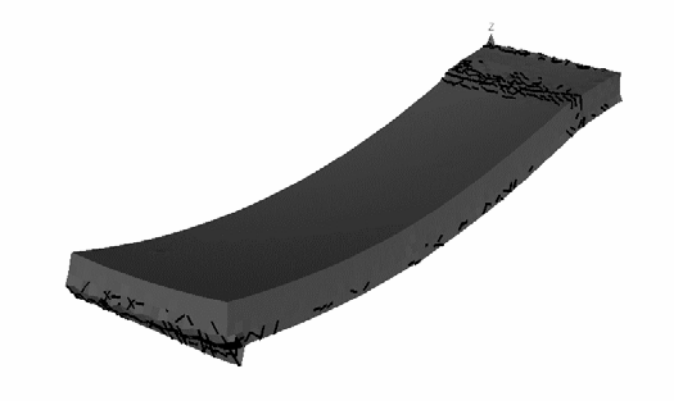

Figure 13. Deformed shape of the 3D finite element model.

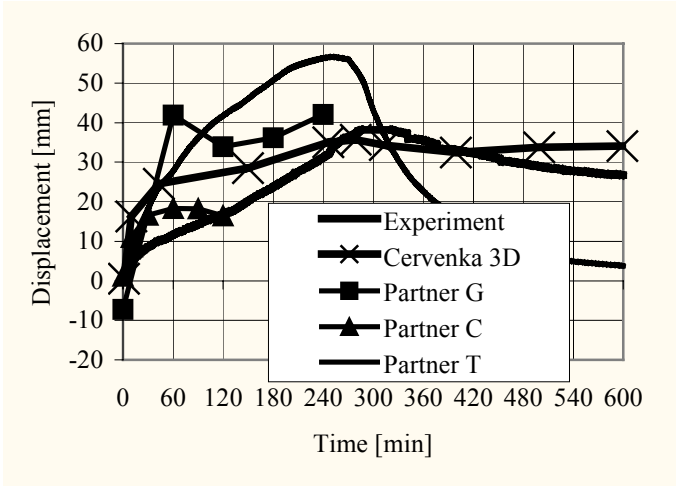

Figure 14. Midspan deflection during the experiment and comparison with numerical predictions.

Figure 15. Photo from the experiment showing an extensive damage at the ceiling corners.

In this work, no experimental data for free thermal strain was available for a given concrete type, therefore the Eurocode 2 formula was used. The free thermal strain had to be reduced by 30% to obtain a better agreement with the measured data. Figure 14 includes also results from other models and other partners on the UPTUN project. These results were typically obtained by a two-dimensional thermal analysis of the slab cross-section, which was later used in an incremental plastic analysis with 2D beam elements.

The final crack pattern is shown in Figure 13, which indicates the formation of a plastic joint on the right side near the vertical hanger. The extensive cracking at the top surface indicates the location of this joint. The joint forms early on during the analysis. The slab is designed such that it cannot withstand the negative bending moment at the vertical hanger, if the slab edges lift upward. This lifting occurs due to the heating of the bottom surface.

Extensive cracking was also calculated along the bottom surface and at the front corner. The results from the 3D analysis show an additional bending in the cross-wise direction, causing the lifting of the slab corners. This lifting caused an excessive damage to the concrete due to escaping flames and smoke.

The structure suffered extensive damage, but full collapse was not reached in the investigated time period neither in the experiment nor in the numerical study.

7 APPLICATION TO VIRGOLO TUNNEL TEST

A real scale fire test was carried out on the 17th February 2005 in Bolzano/South Tyrol – Italy in a tunnel of the Brenner motorway-AG (Virgolo tunnel).

The experimental program was rather extensive. It tested human response, fire detection and suppression systems as well as material and structural behaviour. Six fire resistance shotcrete mixes were tested in order to evaluate their effectiveness as fire protection barriers to the structural concrete. The large-scale test was supplemented by laboratory experiments of the shotcrete specimens. A numerical simulation using the presented material models supported the experimental program. The results from the laboratory tests were used to calibrate the thermal properties of the shotcrete types. The obtained material laws were then used to simulate the behaviour of a tunnel wall protected by the tested materials. The main goal was to qualitatively evaluate the damage to tunnel lining and compare it to the damage of an unprotected wall.

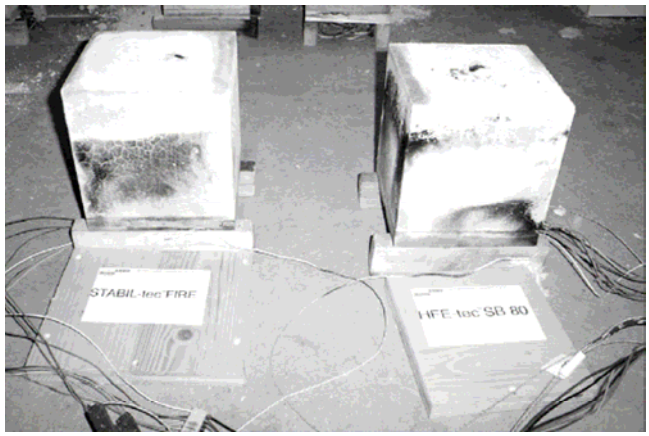

Figure 16. Specimens for laboratory tests

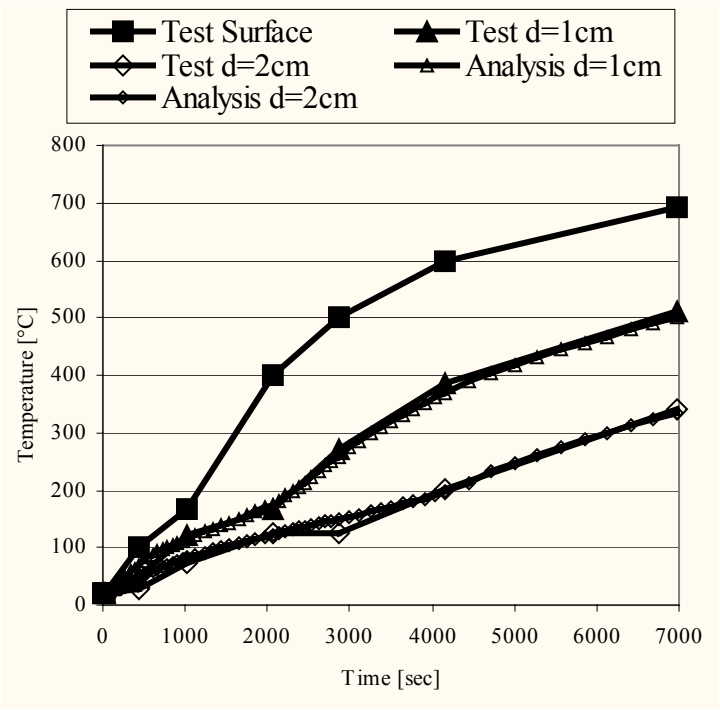

Figure 17. Temperature evolution in shotcrete material for different depths d during the laboratory test

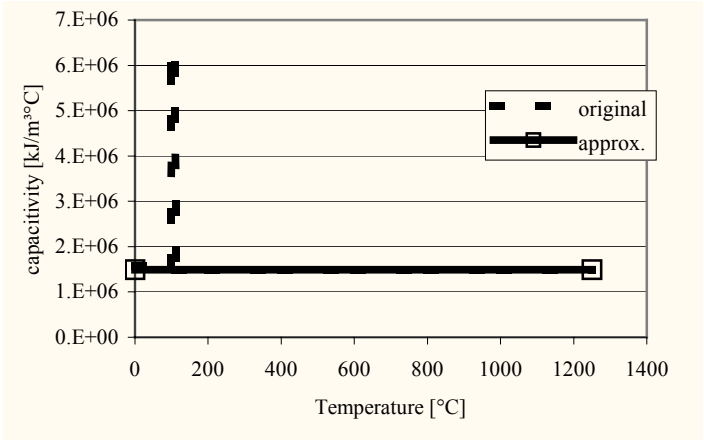

Figure 18. Capacity for the shotcrete material determined by the inverse analysis of laboratory test data.

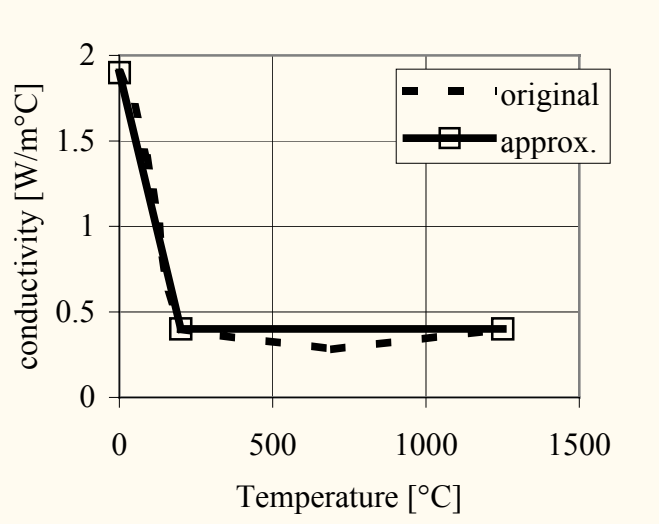

Figure 19. Conductivity for the shotcrete material determined by the inverse analysis of laboratory test data.

Figure 16 shows the geometry of the laboratory specimens. The specimens were cubes with side of 20 cm. One side of these specimens was subjected to a fire load of up to 12kW using gas burners. The temperature was measured at various depths, as is shown in Figure 17 for shotcrete material Meyco© Fix Fireshield 1350 from DEGUSSA. Numerical thermal analysis with ATENA was then used to determine optimal temperature dependent laws for capacitivity and conductivity in order to match the experimental temperature evolution. Probabilistic methods were used (Strauss et. al. 2004, 2006) to find the optimal fit with experimental data (see Figure 17). The final evolution law for capacitivity and conductivity is shown in Figure 18 and Figure 19 respectively.

Subsequently these parameters were used to model the shotcrete performance in a real tunnel scenario.

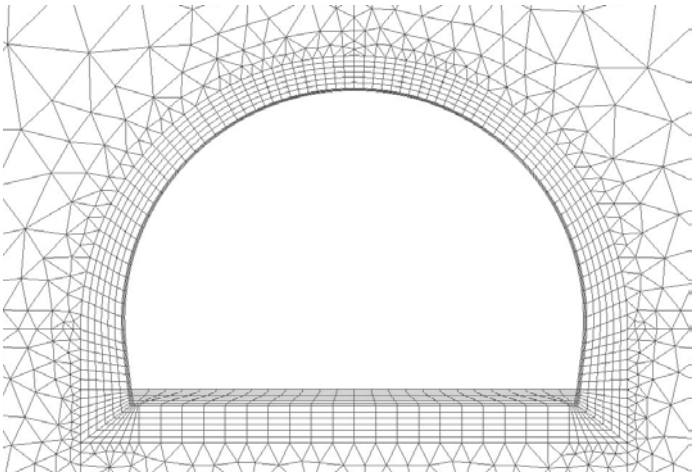

Figure 20. Numerical model for Virgolo tunnel numerical analyses.

The model shown in Figure 20 was subjected to a modified hydrocarbon fire of up to 1300°C. In the interior of the tunnel a 50 mm layer of shotcrete material was applied. The shotcrete layer was modeled by 4 finite elements while for the tunnel lining 7 elements were used through its thickness. The tunnel wall was made of concrete class C25/30 using Eurocode 2 classification.

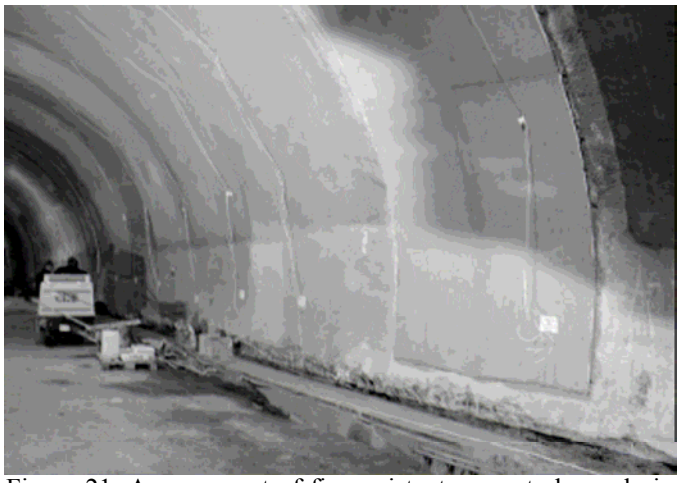

Figure 21. Arrangement of fire resistant concrete layer during the Virgolo tunnel test.

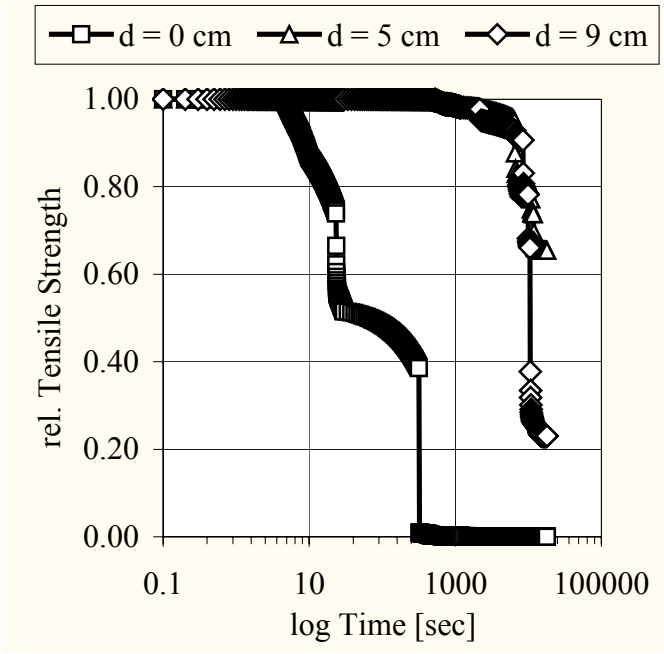

Figure 22. Tunnel wall degradation due to high temperature at various depths

Table 1. Temperature criteria and optimal shotcrete thickness

Location	Criteria	Value
50 mm (concrete-shotcrete interface)	300 °C	214 °C
90 mm (reinforcement depth)	250 °C	141 °C
Optimal shotcrete layer thickness	---	30 mm

Figure 22 describes the evolution of concrete degradation at various depths. The degradation is described as a relative value of concrete strength. The value of 1 indicates original concrete strength, i.e. no damage. The value of zero corresponds to fully damaged material with zero strength.

Table 1 summarizes the main results for the given shotcrete type (i.e. Meyco© Fix Fireshield 135). The recommended design criteria are such that the

temperature at the interface between the fire protection layer and original concrete wall should not exceed 300°C, and the temperature at the depth of reinforcement location should remain below 250°C. Table 1 shows that both criteria are satisfied for the given material, and optimal thickness of the protective layer was determined by a parametric study to be 30 mm.

8 DISCUSSION, CONCLUSIONS AND ACKNOWLEDGEMENTS

The paper presents an extension of the combined fracture-plastic model developed previously by the authors (Cervenka, J. et. al. 1998, 2006). The selected material parameters are made temperature dependent. This allows the model to be applied for the simulation of reinforced concrete structures subjected to fire. The model behavior is demonstrated on simple uniaxial tests that show the model response under various uniform temperature distributions.

The results of a large-scale fire test of a tunnel suspended ceiling were used to verify the model applicability for solving complex structures subjected to fire.

The last section contains an application to real life scenario, where a structural damage due to fire is evaluated using an example of the Virgolo tunnel fire test.

The presented work was part of a European research project UPTUN GRID-CT-2002-00766. The development of reinforcement modeling and temperature dependent material laws was supported by the research projects 103/04/2083, and 103/07/1660 from Czech Grant Agency. The financial support from European community and Czech Grant Agency is greatly appreciated.

REFERENCES

ATENA 2005. *Program Documentation*, Cervenka Consulting, Prague, Czech Republic, www.cervenka.cz

Bažant, Z.P. & Oh, B.H. 1983. Crack band theory for fracture of concrete, *Materials and Structures*, 16, 155-177.York, 360 pp.

Castillo, C. & Durani, A.J. 1990. Effect of transient high temperature on high-strength concrete, ACI Materials Journal, v 87 n 1, p 47-53.

Gawin, D., Pesavento, F., Schrefler, B.A. 2003. Modelling of hygro-thermal behaviour of concrete at high temperature with thermo-mechanical and mechanical material degradation, CMAME, 192, 1731-1771.

Cervenka, J., Cervenka, V., Eligehausen, R. 1998. Fracture-Plastic Material Model for Concrete, Application to Analysis of Powder Actuated Anchors, *Proc. FRAMCOS 3*, 1998, pp 1107-1116.

Cervenka, J., Surovec, J., Kabele, P., 2006, Modelling of reinforced concrete structures subjected to fire, Proc. EuroC-2006, ISBN 0415397499, pp 515-522

de Borst, R. 1986. *Non-linear analysis of frictional materials*, PhD Thesis, Delft University of Technology.

Eurocode 2. 1992-1-2. *Design of concrete structures, Part 1.2. General rules - Structural fire Design*. Draft prENV 1992-1-2.

Jendele, L. 2001. Atena Pollutant Transport Module - Theory. Prague: Edited PIT, ISBN 80-902722-4-X

Jendele, L., Cervenka, V., 2006. A General Form of Dirichlet Boundary Conditions Used in Finite Element Analysis. Paper 165, *Proc. Eighth International Conference on Computational Structures Technology*, ed. B.H.V. Topping, G. Montero, and R. Montenegro. 2006, Civil Comp Press: Las Palmas. 373-374

Hordijk, D.A. 1991. *Local Approach to Fatigue of Concrete*. Ph.D. Thesis, Delft University of Technology, The Netherlands.

Menetrey, P. & Willam, K.J. 1995. Triaxial failure criterion for concrete and its generalization. *ACI, Structural Journal*, 92(3), pp 311-318.

Strauss, A., Bergmeister, K., Novak, D. & Lehky, D., 2004a, Stochastic parameter identification of structural concrete for maintenance, in german, *Beton und Stahlbetonbau*, Vol. 99, No. 12, Vienna, Austria, pp. 967-974

Strauss, A., Bergmeister, K., Lehky, D., & Novak, D., 2006, Inverse statistical nonlinear FEM analysis of concrete structures, *Proc. Comp. Modell., Concrete Structures, EuroC-2006*, eds. Meschke, de Borst, Mang & Bicanic, ISBN 0 415 39749 9, pp. 897-904

Wood., W.L. 1990. Practical-Time Stepping Schemes. Oxford: Clarenton Press.